

## **Bifacial Photovoltaic Technology: Recent Advancements, Simulation and Performance Measurement**

Aghaei, Mohammadreza ; Korevaar, Marc; Babal, Pavel; Ziar, H.

**DOI**

[10.5772/intechopen.105152](https://doi.org/10.5772/intechopen.105152)

**Publication date**

2022

**Document Version**

Final published version

**Published in**

Solar Radiation - Measurement, Modeling and Forecasting Techniques for Photovoltaic Solar Energy Applications

**Citation (APA)**

Aghaei, M., Korevaar, M., Babal, P., & Ziar, H. (2022). Bifacial Photovoltaic Technology: Recent Advancements, Simulation and Performance Measurement. In *Solar Radiation - Measurement, Modeling and Forecasting Techniques for Photovoltaic Solar Energy Applications* IntechOpen. <https://doi.org/10.5772/intechopen.105152>

**Important note**

To cite this publication, please use the final published version (if applicable). Please check the document version above.

**Copyright**

Other than for strictly personal use, it is not permitted to download, forward or distribute the text or part of it, without the consent of the author(s) and/or copyright holder(s), unless the work is under an open content license such as Creative Commons.

**Takedown policy**

Please contact us and provide details if you believe this document breaches copyrights. We will remove access to the work immediately and investigate your claim.

# We are IntechOpen, the world's leading publisher of Open Access books Built by scientists, for scientists

5,800

Open access books available

143,000

International authors and editors

180M

Downloads

Our authors are among the

154

Countries delivered to

TOP 1%

most cited scientists

12.2%

Contributors from top 500 universities



WEB OF SCIENCE™

Selection of our books indexed in the Book Citation Index  
in Web of Science™ Core Collection (BKCI)

Interested in publishing with us?  
Contact [book.department@intechopen.com](mailto:book.department@intechopen.com)

Numbers displayed above are based on latest data collected.  
For more information visit [www.intechopen.com](http://www.intechopen.com)



# Bifacial Photovoltaic Technology: Recent Advancements, Simulation and Performance Measurement

*Mohammadreza Aghaei, Marc Korevaar, Pavel Babal and Hesam Ziar*

## Abstract

In this chapter, we introduce the physic principle and applications of bifacial PV technology. We present different bifacial PV cell and module technologies as well as investigate the advantages of using bifacial PV technology in the field. We describe the measurement and modeling of Albedo, which is one of the important factors for the energy yield of bifacial PV technology. For an accurate assessment of the performance ratio of bifacial PV strings, it is necessary to measure the albedo irradiance using an albedometer or the front- and rear-side plane of array (POA) irradiance. We also discuss the advanced techniques for the characterization of bifacial PV modules. By means of simulation, we give insight into what boundary conditions result in new bifacial technology gains and the influence of the mounting position of irradiance sensors. We executed several simulations by varying the sensor positions on the rear side of the PV modules, different places, different albedo numbers, mounting heights, different geographical locations with various tilts, seasons, and weather types. To validate the simulation results, we performed various experiments in the field under different conditions. The results prove that the bifacial gain is highly dependent on the mounting heights of PV modules, tilt angles, weather conditions, latitude, and location.

**Keywords:** bifacial photovoltaics (PV) technology, bifacial solar cell, bifacial PV module, bifaciality factor, solar radiation, Albedo

## 1. Introduction

In recent decades, photovoltaics (PV) technology has received more attention and PV installation is being dramatically deployed. The PV capacity has been exceeded from one Tera Watt (TW) in the world, which was an impressive milestone in solar energy sector [1]. A novel development is the advent of bifacial PV modules that enhance energy production by converting incident irradiance on the rear side of the module into electricity.

Bifacial solar photovoltaics (PV) cells as a promising technology convert the photons from albedo and incident irradiance into electricity [2]. The bifacial solar PV cell collects the photons simultaneously from both its front and rear sides, whereas the monofacial solar cells can only convert the incident irradiance on the front side [3–5]. The bifacial PV technology as a novel approach to generating electricity with higher performance was investigated by many research groups over

five decades [6, 7]. This technology was first applied to the satellites by Russia [2]. In 1970s, Mexican and Spanish researchers released their progress results of bifacial solar cells [8, 9]. Other Spanish research groups obtained the high efficiency and power gain for bifacial PV cells in 1980s [10–12]. In 2000s, the bifaciality concept was introduced for several applications, namely, noise barrier fences and shades [13]. In recent decades, bifacial PV technology has been more considered commercially. In this regard, various companies, such as Yingli Solar, bSolar, Sanyo, and PVG solutions, have produced the bifacial PV modules [14] with different crystalline silicon (c-Si) bifacial PV cell structures, such as PERC (passivated emitter rear contact), PERL (passivated emitter rear locally diffused), PERT (passivated emitter rear totally diffused), IBC (interdigitated back contact), and HIT (heterojunction with intrinsic thin layer).

Bifacial PV modules aim to improve the energy output of PV systems. This is because of doubling the power output of PV through collecting both direct and albedo radiation. Therefore, the bifacial solar cells increase the power density of PV modules [15]. As a result, the PV module and balance of system (BOS) costs and levelized cost of energy (LCOE) are reduced [16].

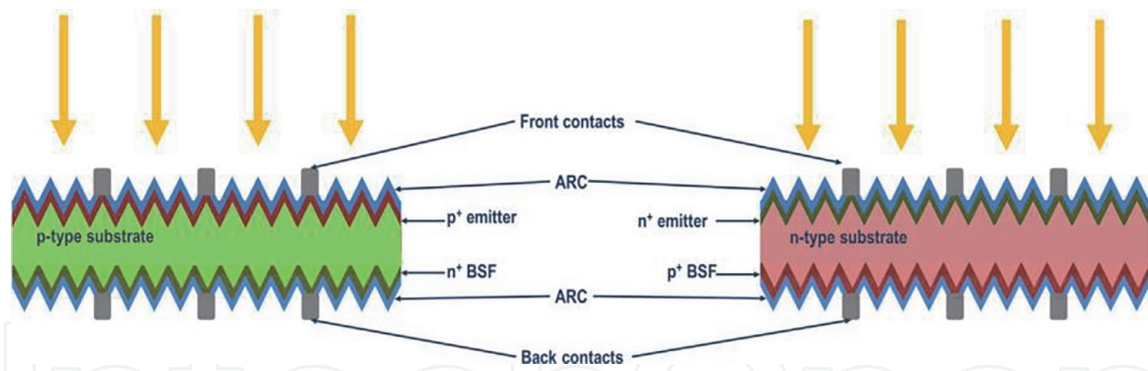
To date, several large-scale PV power plants were developed using the bifacial c-Si PV modules. For example, a bifacial PV power plant with a capacity of 1.35 MWp was installed in Hokuto city, Japan. The performance data of this plant demonstrated a 21.9% gain compared to a monofacial PV plant with an identical capacity [17]. **Table 1** summarizes the details of some bifacial PV power plants installed around the world.

The cell working temperature is decreased in bifacial solar cells compared to monofacial ones resulting in maximizing the power output [18, 19]. However, the combination of irradiance effect on both front and rear sides of bifacial PV cells resulting a complexity to characterize both sides simultaneously under standard test conditions (STC 1000 W/m<sup>2</sup>, AM 1.5 spectrum, and ambient temperature of 25°C). **Figure 1** depicts a scheme of standard bifacial crystalline silicon solar cells. As illustrated in **Figure 1**, an open metallization grid is printed on the front and rear sides of the bifacial structure to be able to collect the incident irradiance from both sides. In n-type bifacial cells, the back surface field (BSF) is  $n^+$ , whereas the  $p^+$  diffused layer serves as the emitter, contrary to the p-type bifacial solar cells. The texturized wafers and passivating anti-reflective coatings (ARC) are partially covered by screen-printed metallic contacts to achieve the open metallization grid [19].

Location	Module technology	PV Plant capacity (MWp)	Annual energy production (GW h)
San Felipe, Chile	Megacell, n-type BiSoN module (BiSoN cell)	2.48	5.78
Eastern US	Sunpreme, GxB370W (Hybrid Cell Technology—HCT)	12.8	8
Hokuto, Japan	PVG Solutions, EarthON 60 (EarthON cell)	1.35	1.47
Datong City, Shanxi, China	Yingli Solar, n-type PANDA module (n-Pasha cell)	50	80
Golmud, China	LONGI Solar	20	—
Golmud, China	Trina Solar	20	—
Golmud, China	Jinzhou Yangguang Energy	20	—
Golmud, China	JA Solar	11	—

**Table 1.**

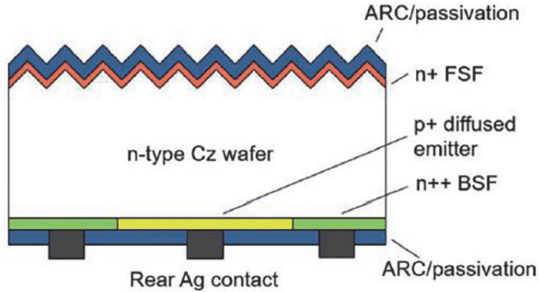
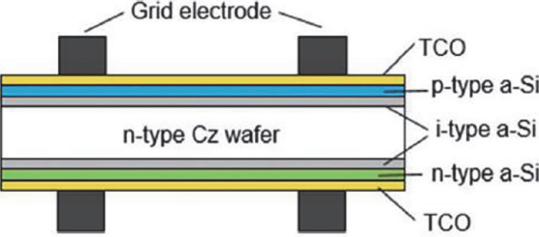
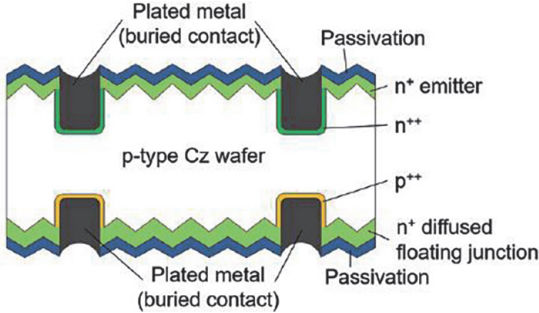
*The list of bifacial PV power plants using crystalline silicon (c-Si) bifacial modules [8].*

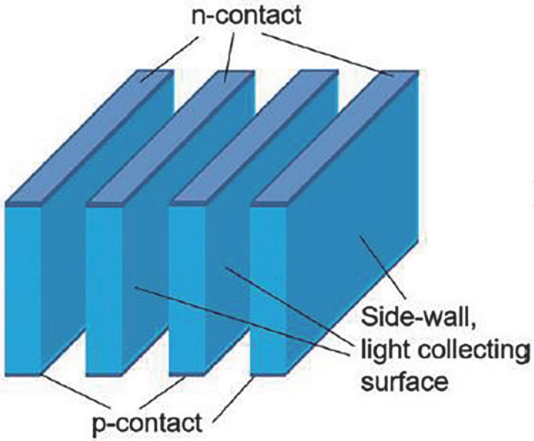
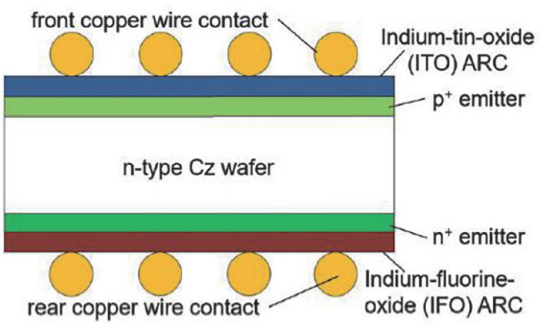


**Figure 1.** Standard n-type and p-type bifacial crystalline silicon solar cells [2].

**Table 2** summarizes different c-Si bifacial PV cell technologies, including the cross-sectional schematics of each bifacial PV cell structure as well as the efficiency and bifaciality of some cell technologies.

c-Si cell technology	Description	Schematic of the cell structure
Bifacial PERC	<ul style="list-style-type: none"> <li>Acronym for passivated emitter rear contact</li> <li>Efficiency: 19.4–21.2% (front), 16.7–18.1% (rear) [20, 21]</li> <li>Bifaciality: 80% [20]</li> <li>Mainly based on p-type crystalline silicon (c-Si) wafer</li> <li>The cell structure was used for studying the Shockley–Read–Hall recombination velocity at the Si–SiO<sub>2</sub> interface [22] between 1988 and 1991</li> <li>It was introduced as a new bifacial PV cell in 1996 [21]</li> <li>ISF Hamelin [20] and SolarWorld [23] demonstrated the industrial bifacial PERC (or PERC+) design for mass production</li> </ul>	
PERL	<ul style="list-style-type: none"> <li>Acronym for passivated emitter rear locally diffused</li> <li>Efficiency: 19.8% (front) [24]</li> <li>Bifaciality: ≥89% [24]</li> <li>Mainly based on p-type c-Si wafer</li> <li>Boron is locally diffused into contact areas at the rear side [25]</li> </ul>	
PERT	<ul style="list-style-type: none"> <li>Acronym for passivated emitter rear totally diffused</li> <li>Efficiency: 19.5–22% (front), 17–19% (rear) [26–28]</li> <li>Bifaciality: ≥85% [26, 29]</li> <li>Commercialized based on the n-type c-Si wafer; also based on p-type</li> <li>PVGS developed n-type EarthOn cell in 2009 [29]</li> </ul>	

c-Si cell technology	Description	Schematic of the cell structure
IBC	<ul style="list-style-type: none"> <li>• ECN developed n-Pasha (passivated all-sides H-pattern) cell to reduce yield loss; it was commercialized by Yingli Solar as PANDA [26]</li> <li>• N-MWT (Metal Wrap Through) was also proposed by ECN to narrow down busbars and reduce metal coverage</li> <li>• ISC Konstanz developed BiSoN cell and commercialized by MegaCell</li> </ul>	
HIT	<ul style="list-style-type: none"> <li>• Acronym for heterojunction with intrinsic thin-layer</li> <li>• Efficiency: 24.7% [36]</li> <li>• Bifaciality: ≥95% [37]</li> <li>• Mainly based on n-type c-Si wafer</li> <li>• Introduced by Sanyo (now Panasonic) in 1997 and entered into the serial production under the brand name HITs [36, 38]</li> <li>• Bifacial HITs cell was introduced by Sanyo (now Panasonic) in 2000 and entered the serial production</li> <li>• Basic technology patent was discontinued and opened to the public in 2010; Meyer Burger adopted the cell Technology [39]</li> </ul>	
DSBCSC	<ul style="list-style-type: none"> <li>• Acronym for double-sided buried contact solar cell</li> <li>• Efficiency: 22% [40, 41]</li> <li>• Bifaciality: 74% [42]</li> <li>• Plated metal contact is entrenched in the laser-formed groove</li> <li>• Low resistance and low shading losses, due to high</li> </ul>	

c-Si cell technology	Description	Schematic of the cell structure
	metal aspect ratios and lightly diffused emitter [40]	
Silver	<ul style="list-style-type: none"> <li>Developed at the Centre for Sustainable Energy Systems, Australian National University [43]</li> <li>Efficiency: 19.4% [43]</li> <li>Narrow grooves are created via conventional micro-machining technique, forming a series of thin silicon strips [44]</li> <li>Reduces silicon consumption by up to a factor of 10 [44]</li> </ul>	 <p>A 3D perspective diagram of a bifacial cell structure. It shows a series of parallel, thin silicon strips. The top surface of each strip is labeled 'n-contact' and the bottom surface is labeled 'p-contact'. The vertical surfaces between the strips are labeled 'Side-wall, light collecting surface'.</p>
BICONTY	<ul style="list-style-type: none"> <li>Acronym for bifacial concentrator n-type</li> <li>Efficiency: 17.6% (front), 16.7% (rear) [45]</li> <li>Based on the laminated grid n-type solar cell [45]</li> <li>Silver free—uses copper wire coated with low-temperature solder, resulting in very low shadow loss and resistance loss [45]</li> </ul>	 <p>A cross-sectional diagram of a BICONTY bifacial cell. From top to bottom, the layers are: front copper wire contact (yellow circles), Indium-tin-oxide (ITO) ARC (blue layer), p+ emitter (green layer), n-type Cz wafer (white central layer), n+ emitter (green layer), rear copper wire contact (yellow circles), and Indium-fluorine-oxide (IFO) ARC (red layer).</p>

**Table 2.**  
 Summary of c-Si bifacial PV cell technologies [8].

In recent years, the bifacial module technology gets more attention in the PV market and numerous attempts have been devoted to the standardization, niche applications, characterization techniques as well as industrial production and costs. The worldwide growth of c-Si bifacial PV cells and modules is predicted by the International Technology Roadmap for Photovoltaic (ITRPV) and it is expected that the bifacial PV technology (c-Si) will be increased by more than 35% by 2028 [46].

## 2. Albedo: measurement and modeling

Albedo as an important input for the surface energy balance equation [47], thus affects the surface temperature. The speed of chemical and biological reactions is increased due to heat. To overcome this, soil (as a surface) temperature is used to predict the rate at which processes such as seed germination occur. Furthermore, erosion rate and the water content of the soil depend on the ground albedo [48, 49]. This makes albedo utter importance for different environmental processes (e.g., food production) [49]. The local albedo is an influential factor in the heat-island formation that affects public health, namely, air quality and greenhouse gas concentration [50]. Moreover, the energy usage during warm seasons by occupants is related to the value of local albedo [49]. Furthermore, albedo directly influences the electric energy generated by the PV system. Therefore, knowledge about albedo is significant for accurate yield predictions for PV systems, resulting in minimizing technical risks and

cost as well as enhancing service life. However, albedo has received less attention so far due to its complexity and minor share in irradiation stroked on a surface of a monofacial PV module. In this regard, albedo is either neglected [51] or assumed to be a constant value [52] in the modeling of PV systems. However, nowadays there are increasing trends of bifacial PV installations and urban PV integration [53], where albedo's contribution to electrical yield becomes more significant [54, 55]. Therefore, better understanding, precise measurements, and accurate estimation of albedo are of utter importance and should be further considered.

## 2.1 Albedo

Surface albedo<sup>1</sup> is a unitless variable defined as the ratio of the solar radiation at a certain wavelength range reflected from a particular surface (upwelling) to the solar incident upon it.

$$\alpha = \frac{\Phi_S^{\text{downward}}}{\Phi_S^{\text{upward}}} \quad (1)$$

where  $\alpha$  is surface albedo,  $\Phi_S^{\text{down}}$  and  $\Phi_S^{\text{up}}$  are the incoming global radiant fluxes (W) on the down-facing and up-facing sides of the surface S, respectively. Albedo and reflectance are not the same, although often interchangeably used or even misinterpreted. Surface albedo is an angular and spectral integrated value of the spectral bidirectional reflectance distribution function (BRDF):

$$BRDF_\lambda = \rho(\theta_i, \phi_i, \theta_r, \phi_r, \lambda) = \frac{L(\theta_i, \phi_i, \theta_r, \phi_r, \lambda)}{E(\theta_i, \phi_i, \theta_r, \phi_r, \lambda)} \quad (2)$$

where BRDF is the ratio of observed radiance  $L$  to incident irradiance  $E$  at a wavelength  $\lambda$  under certain viewing geometry ( $\theta_i$  and  $\phi_i$  are, respectively, zenith and azimuth angles at the incident direction;  $\theta_r$  and  $\phi_r$  represent zenith and azimuth angles, respectively, at the observing direction). Albedo (as a measure used in energy calculations) is normally shown with the Greek letter  $\alpha$ , while reflectance (as a property of a material) function is shown by  $\rho$ .

Albedo becomes important in the surface energy balance since radiation contains energy. Therefore, it plays a key role in the regulation of earth's surface energy budget [56]. For a piece of land, surface albedo is highly variable, both spatially and temporally. Variations in land coverage and surface conditions, such as snow [57], vegetation [58], urbanization [59], soil moisture [60], sky condition, and position of the Sun, (such as cloudiness [61]), change surface albedo significantly. Thus, surface albedo not only depends on the surface features but also on almost everything that forms the surrounding of surface. In simple terms, at every instant of time, albedo depends on three key factors, namely, material, light source features, and geometry<sup>2</sup> [62].

## 2.2 Albedo measurement (in situ and satellite)

Albedometer consists of two back-to-back mounted pyranometers and is used for in situ measurements of local albedo. The upper sensor measures the incident global solar radiation and the sensor at the bottom side measures the solar radiation reflected from the surface (s) below. Dividing the obtained value from the bottom

<sup>1</sup> Albedo in Latin means whiteness, introduced by Johann Heinrich Lambert in 1760.

<sup>2</sup> Here means arrangement of the surrounding objects in a three-dimensional space.



sensor by that from the upper one gives the value of the albedo at a certain location and time [63]. **Figure 2a** depicts a real albedometer and its schematic is illustrated in **Figure 2b**. The view factor from the albedometer to the target surface makes an influence on the measurement result; hence, the correct distance from the target surface should be opted. Besides, one instant measurement usually does not give the correct average value of albedo, since albedo changes over time. Therefore, long-term measurements of albedo are required. Moreover, the shadow casted by the albedometer itself can reduce the accuracy of the measurement due to the irradiance impinging on the target surface will be different from the incident irradiance on the top pyranometer. The influence of the albedometer shadow on the measurement accuracy depends on the view factor from the albedometer to its shadow [64]. Typically, it is suggested to run albedo measurements during cloudy days to reduce this effect [62]. However, while assessing albedo for larger areas and broader scales is of interest, satellite data are often processed, namely, MODIS (Moderate Resolution Imaging Spectroradiometer) instrument on EOS Terra satellite is used to remotely sense the land albedo of regions on earth.

Satellite albedo data usually have high resolution (in a range of Km). The satellite scans a region on earth once every one or two days [65]. Since albedo is changed over time, hence by the time that a satellite passes over a region on earth and records the albedo, the recorded value may not represent the mean land albedo of the targeted region. However, repeating this procedure for decades gives vital indications of albedo trends for a specific region on earth.

Satellites observe a combined result of the atmosphere and land surface interactions. Therefore, surface albedo is typically retrieved from multispectral optical data considering the viewing geometries. There are common approaches and algorithms used for estimating land surface albedo from satellite optical data. This comprises three following steps—(i) atmospheric correction to filter out the effect of the atmosphere, (ii) BRDF modeling to account for the reflectance anisotropy effect of the land surfaces, and (iii) narrowband to broadband conversion to obtain broadband albedo from spectral albedos, which is available only at certain satellite measurement channels [66].

### 2.3 Local Albedo models

Most of the local albedo models have been developed between 60's and 90's. The local albedo models rely on empirical coefficients based on long-term data measurements. By the end of 90's, first albedo observing satellites that were orbiting

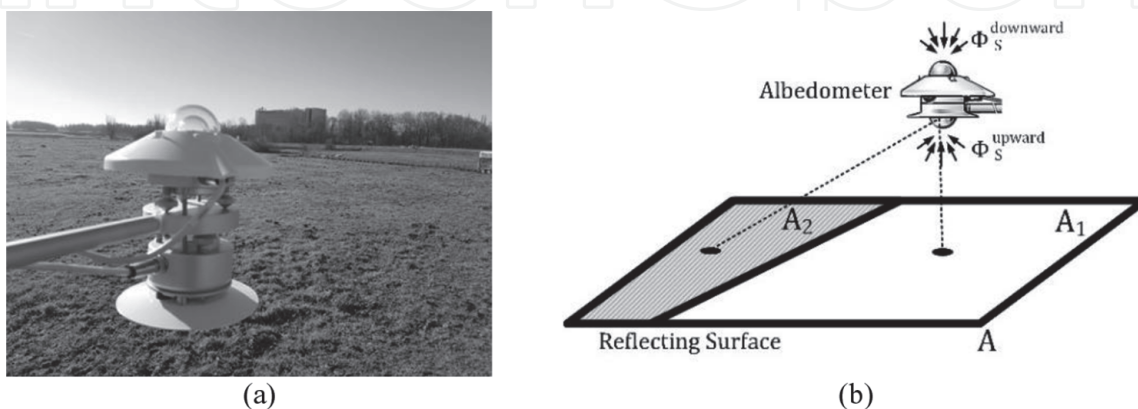


**Figure 2.**  
(a) A real albedometer installed on a grass field during landscape survey for photovoltaic installation, and (b) simple schematic of albedometer placement. If the albedo surface  $A_1$  is of interest, surface  $A_2$  will also make an influence on the measurement.

the earth shifted the attention of researchers to the development of algorithms for albedo retrieval from satellite data [67]. However, satellite-derived albedos do not offer enough resolution for complex topography with highly spatial variations, such as in urban areas, where micro-climates and sustainable energies are hot topics [68, 69]. Here, we have reviewed the main local albedo models.

The simplest albedo models are the constant albedo assumption and mean measured albedo, which, respectively, suggest that constant albedo of  $\alpha = 0.2$  and  $\alpha = \alpha_{\text{site}}$  can be applied to all the sites [70, 71]. The constant albedo model may include a considerable error in different situations. The mean measured albedo model demands long-term monitoring of albedo for each site, which is practically impossible.

Another albedo model is the zonal albedo model, which works based on polynomial expressions for the latitude range of  $20^\circ < \varphi \leq 60^\circ$  in North America:  $\alpha = \sum_{i=1}^{i=3} \alpha_i \varphi^i$ , ( $\varphi$  is in degrees). The empirical coefficients ( $\alpha_i$ ) are determined monthly and have been presented in ref. [72]. The drawback of this model is that it cannot be used for local albedo estimation and only is valid for North America. Next model is the *Nkemdirim model* [73], which describes albedo as a function of solar elevation:  $\alpha = \alpha_0 \exp(b \cdot \theta_z)$ , where  $\theta_z$  is the solar zenith angle in degrees, and  $\alpha_0$  and  $b$  are site-dependent coefficients based on the ground characteristics that should be measured for each location. For this model, the accuracy is dependent on the in situ estimated coefficients. *Beam/diffuse albedo* as a more advanced model separates albedo into its beam ( $\alpha_b$ ) and diffuse components ( $\alpha_d$ ), as:  $\alpha = f(\alpha_b, \alpha_d)$ . This modeling approach requires site-dependent coefficients, which must be determined experimentally for every site [74].

One of the most widely used albedo models is based on the *isotropy assumption*. This model theoretically outputs the albedo using:  $\alpha = 0.5 \cdot \alpha_1 (1 - \cos \beta)$ , where  $\alpha_1$  denotes the albedo coefficient of the site and  $\beta$  is the tilt angle of the surface [75]. This model cannot distinguish the albedo difference for times with equal amounts of global horizontal irradiance and only can consider different values of direct and diffuse components. In this model, the empirical factor of  $[1 + \sin^2(Z/2)] / |\cos \theta|$  is applied as a correction factor for anisotropy of the surface reflection [76], which is called *Temps and Coulson model*.

A more sophisticated model that does not need empirical coefficients has been developed based on the roughness of the surface and the geometry of the surrounding, reflectivity of the materials, and the sky condition. All these parameters are fed into one coherent equation:  $\alpha = \sum R_i [C_i \cdot F_{S \rightarrow Ai1} + (1/(H+1))(C_i \cdot F_{S \rightarrow Ai1} + F_{S \rightarrow Ai2})]$ , where  $R$  is the spectral reflectivity of the materials forming the surface,  $F_{S \rightarrow Ai1}$  and  $F_{S \rightarrow Ai2}$  are, respectively, the view factors from the albedometer to the sunny and shaded parts of the target surface.  $H$  is a coefficient dependent on the position of the Sun and the beam and diffuse components of the sunlight.  $C_i$  and  $C_i'$  are probability-based coefficients calculated by knowing the roughness of the target surface. This model provides better accuracy compared to other local albedo models. This model does not require an empirical coefficient, and also mathematically proves albedo of a surface is always lower than or equal to its reflectivity ( $\alpha \leq R$ ) [62].

### 3. Indoor characterization of bifacial PV module

For the characterization of bifacial PV modules, the definition and regulation of Standard Test Conditions (STC; 1000 W/m<sup>2</sup> Global irradiance, AM1.5G spectral irradiance, and cell temperature at 25°C) should be extended to consider the

spectral and irradiance on rear and front sides of PV modules. In 2019, IEC TS-60904-1-2 was prepared to address the requirements for the characterization of bifacial PV modules [77].

### 3.1 Single-light source

The single-sided (separate) measurement under STC is a method for indoor characterization of bifacial PV modules, as described by the following equations. In the first step,  $BiFi_{I_{sc}}$  is computed according to Eq. (3) [78]:

$$BiFi_{I_{sc}} = \frac{I_{sc,rear}}{I_{sc,front}} \quad (3)$$

This equation represents the ratio of the short-circuit currents for the front and rear sides of bifacial PV modules. Then  $BiFi_{I_{sc}}$  is applied in Eq. (4) to calculate the bifacial equivalent irradiance,  $G_E$ :

$$G_E = 1000Wm^{-2} + BiFi_{I_{sc}} \times G_{rear} \quad (4)$$

$G_E$  considers the additional contribution of rear-side irradiance on top of the one Sun front irradiance. Subsequently, the front side of the bifacial PV module is flashed with the higher irradiance level of  $G_E$  to obtain the bifacial maximum power and efficiency [78]. In this method, the unintended current contribution from the non-illuminated side, which is associated with the reflected irradiance from the surroundings to the optical properties of the module, and to the geometrical disposition of the cells, must be avoided. A common practice involves covering the non-illuminated side of the bifacial module with a black mask [79, 80]. The contribution of unintended illumination could still result in 15% increase in maximum power when using the setup with a black curtain as the background and the rear side of the bifacial PV module covered by a black mask. G. Razongles et al. [81] have derived equations to extrapolate the maximum power rating of bifacial PV modules corresponding to the front- and rear-side illumination. The main equations are given as:

$$P_{max}(S) = S \times f \times P_{max} \quad (5)$$

$$S = \frac{G_{front}}{1000} \quad (6)$$

$$f = 1 + a \times (S - 1) + b \times \ln S + c \times (S - 1)^2 + d \times (\ln S)^2 \quad (7)$$

Eqs. (4) and (5) were taken from the PV method. The number of Suns,  $S$ , refers to the ratio between frontside irradiance and the STC value ( $1000 W m^2$ ). Eq. (7) is the polynomial function of the Neperian logarithm;  $a$ ,  $b$ ,  $c$ , and  $d$  are constants. The parameter  $f$  represents the “irradiance coefficient.”  $P_{max}$  is maximum power, which was measured by flashing the front side at an equivalent irradiance, as described in Eq. (8):

$$G_E = G_{front} + G_{back} \times \frac{I_{sc,STC,Back}}{I_{sc,STC,front}} \quad (8)$$

Alternatively, Corbellini et al. [82] calculated the bifaciality factor using the STC power of the front and rear sides, which is expressed in Eq. (9):

$$BiFi_{Pmax} = \frac{P_{max, rear}}{I_{max, front}} \quad (9)$$

Accordingly, the unintended irradiance on the non-illuminated side has been quantified that is included in the single-sided power measurements (STC). It was measured repeatedly using a reference cell at several positions on the non-illuminated side. The irradiance ratio on the positions concerning the irradiance on the illuminated side was calculated. This was also measured by a reference cell. The lowest ratio was taken to correct the power measurements (STC) for both the front and rear sides. Moreover, Singh et al. proposed other equations based on the one-diode equivalent model [83] to calculate the power and efficiency of bifacial PV modules.

### 3.2 A single-light source with reflector or mirrors

Using a reflector that can be located closely behind the rear side of the module, it is possible to obtain the bifaciality of bifacial PV modules. However, a reflective white sheet or background yields irreproducible results. The rear-side illumination condition mostly depends on the reflector properties and light source geometry. Moreover, it depends on the transmittance of the PV cell and module. This probably led to possible difficulties in the quantification of these effects and their standardization [84].

Razongles et al. [81] have used a similar setup (see **Figure 3**) to the Bifacial Cell Tester (BCT) [85]. Soria et al. [86] have conducted bifacial PV mini-module (of four cells) characterization using an identical setup. As shown in **Figure 3**, to reduce the influence of angle, it is possible to optimize the angle between the bifacial PV module and the mirrors (e.g., 44.1° instead of 45°) [86]. Hitherto, this setup has not been scaled up for full-size bifacial PV module characterization.

### 3.3 Double-light source

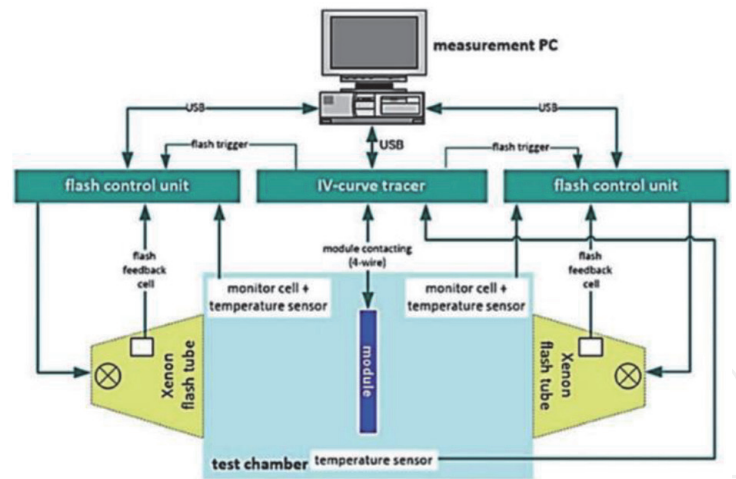
For the characterization of full-size bifacial PV modules, new setups with two light sources have been proposed by industrial partners. For instance, Eternal Sun has proposed a setup including two identical units of the solar simulator (see **Figure 4a**) [81]. In this method, a full-size bifacial PV module is sandwiched between both solar simulators for characterization. In another method, an integrated setup (see **Figure 4b**) with two independently controlled xenon flashers (solar simulators) was proposed by h.a.l.m. elektronik [84]. In this technique, the full-size bifacial PV module (under characterization) is secured inside a test



**Figure 3.**  
*Two-mirror setup for bifacial PV module characterization [81].*



(a)



(b)

**Figure 4.**

(a) A bifacial illumination setup using two identical solar simulators, proposed by Eternal Sun [81], and (b) A bifacial illumination setup proposed by h.a.l.m elektronik [84].

chamber. Theoretically, both solar simulators are controlled simultaneously by a single control system to avoid systematic error due to lagging or mismatch between the flashing sequence of the simulators. It is also possible that illumination on one side of the bifacial PV module will interfere (constructively or destructively) with the illumination on the other side of the module through transmittance and reflection of irradiance between and through cells, thereby introducing irradiance non-uniformity and inconsistencies. A commercial double-light source solution has been proposed by Swiss company Pasan SA (subsidiary of Meyer-Burger Technology AG) by merely doubling its existing multi-lamp Xenon module simulator. In this method, the distance between the two light sources is approximately 16 meters. This helps to reduce the interferences between them.

However, replacing the xenon lamp with LED light led to enabling variation of spectral irradiances [87, 88]. This aims to enhance the prediction of real-world performance or simulate the rear-side irradiance conditions that are probably closer to the diffuse component of AM1.5G than AM1.5G itself (the standard reference irradiance for both front and rear sides of the module, according to the draft version of IEC TS 60904-1-2). The LED-based solar simulator achieving Class AAA has been made commercially available but is yet to be adapted for simultaneous illumination (double-light sources). In summary, the main fundamental challenges would be related to the spatial requirement and the cost of deploying two solar simulators. Therefore, for justification of the measurement results' accuracy, it is recommended to conduct a cost-benefit analysis for the required setup cost.

#### 4. Simulation of bifacial gain for latitude, tilt, and weather

The bifacial gain defines as an additional amount of power generated by a bifacial PV module over a similar monofacial PV module. The amount of bifacial gain depends on many factors, namely, ground albedo, the height of mounted PV module, the ground coverage ratio, the bifaciality factor of the PV module, and the angular distribution of the incident light. This angular distribution changes with the solar position, influenced by the time of day, season, and location on the earth, as

well as by the weather (diffuse cloudy sky as opposed to clear sky). Here, we investigate how big the influence of these factors is on the bifacial gain.

The performance ratio of PV plants with bifacial PV module technology is determined by measuring the plane of array (POA) irradiance and also the irradiance due to ground albedo. Some albedometers (e.g., produced by Kipp & Zonen) can measure either the albedo or the front and rear sides POA, see **Figure 5a**.

Now, the question is that “to what extent does the position of the rear side POA sensor influence the irradiance measurement?” To come to insight into what extent the measurement position influences the irradiance measurement, we have performed a simulation study using “Bifacial Radiance” software [89] on a bifacial PV plant, as sketched in **Figure 5b**. The measurement position has been investigated when it comes to the position on the rear side of fixed PV modules. Additionally, the measurement position for different albedos, locations (and corresponding tilt), the heights of PV module, intra-plant positions as well as month of the year and weather were investigated by several studies [90–92]. The main simulation results of the sensor position are reported in the following sections.

#### 4.1 Simulation method

In this study, the simulations have been executed using “Bifacial Radiance” toolkit that was developed by NREL [89]. This toolkit uses ray-tracing technique to simulate a set of bifacial modules that are either installed on a fixed or a tracking mounting structure. The simulation was run starting at the settings reported in **Table 3**. The general layout is shown in **Figure 5b** to yield the bifacial gain as a function of albedo, height, and location of the site, impacting the tilt angle (here we assumed the tilt angle is equal to the latitude) [93]. The simulation was run to yield the cumulative yearly results. Moreover, the seasonal effect was investigated by selecting certain days and months of the year with different weather conditions. We have imported TMY weather data for the simulation [94].

The simulation was run to yield a distribution of  $POA^{\text{rear}}$  over the rear of the bifacial PV module and to evaluate optimal positions for measuring irradiance. Subsequently, it was investigated how robust is this value by first varying the position within the PV plant. The position was moved from the edge of the PV module toward the center of the row in a set of steps. Secondly the clearance height, albedo was varied over a large range of values. Later, we assessed the effect of the site location and tilt angle [93].

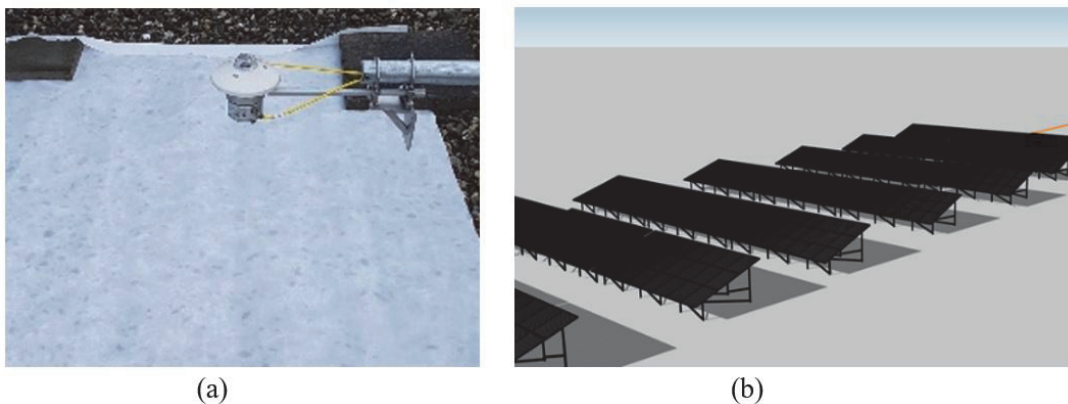


**Figure 5.**

(a) Kipp & Zonen Albedometer mounted above a white surface, and (b) Sketch of bifacial Modules mounted on a fixed mounting structure in seven rows as used in the simulation.

Setting	Value	Setting	Value
Clearance height	0.8 m	Albedo	0.3
No. of sensors	20	Orientation	Landscape
Tilt	25°	Rows	7
Azimuth	180°	No. Modules stacked	4
Plant type	fixed	Modules per row	80
GCR	0.35	Location	Riyadh S.A.

**Table 3.**  
 Simulation settings and parameters of the PV plant in bifacial radiance.

## 4.2 Results

### 4.2.1 Bifacial gain simulation results

**Figure 6a** and **b** shows the simulation results of albedo and clearance height. With an increase in albedo, the bifacial gain is linearly increased. For small clearance heights (i.e., modules mounted close to the ground), the bifacial gain also linearly is increased. However, for larger heights, the changes of bifacial gain would be more constant.

**Figure 7a** and **b** depicts the bifacial gain for a certain time, less than a year for different seasons (1 month) and weather conditions (1 day). The results of bifacial gain for different seasons show that the bifacial gain in summer is significantly higher compared to the bifacial gain in fall or winter.

The weather condition influences the bifacial gain, namely, when the weather is more cloudy then the bifacial gain is increased and vice versa. The seasonal

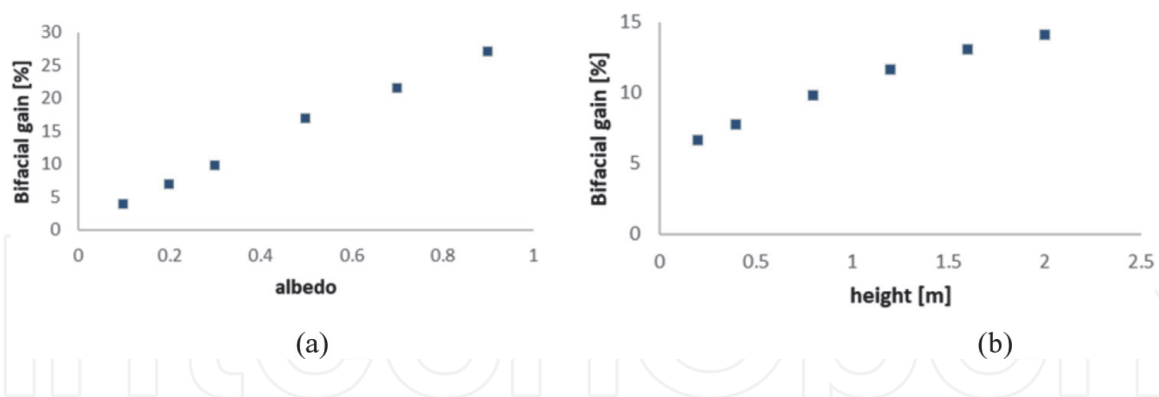


**Figure 6.**  
 Bifacial gain as a function of (a) the albedo and (b) the clearance height.

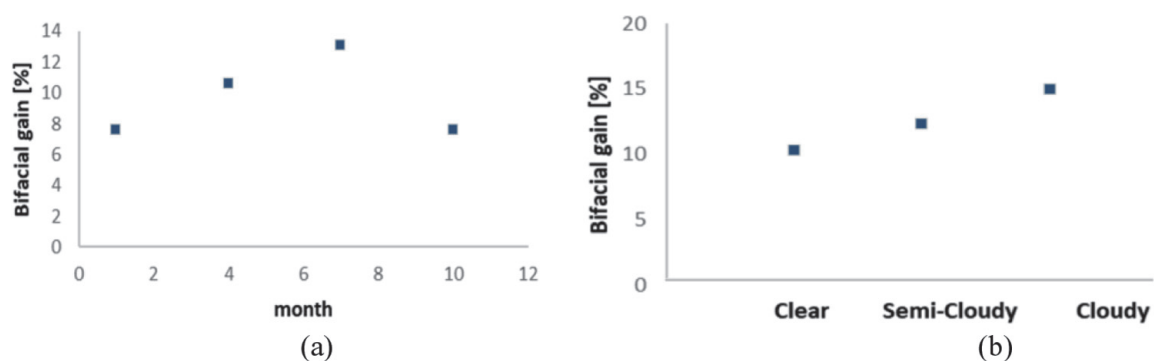


**Figure 7.**  
 Bifacial gain as a function of (a) the season and (b) the weather.

conditions also influence the angular distribution of the irradiance incident on the front and rear sides of the bifacial PV modules.

The bifacial gain as a function of location on the earth and the corresponding tilt angle is shown in **Figure 8**. The higher tilt angles of PV module located at a higher latitude resulted in a higher bifacial gain.

#### 4.2.2 Sensor position simulation results

The cumulative yearly average irradiance on the rear side of the PV modules was calculated using “Bifacial Radiance.” **Figure 9a** shows the results of located bifacial PV modules in the center of the PV plant using the same input listed in **Table 3**.

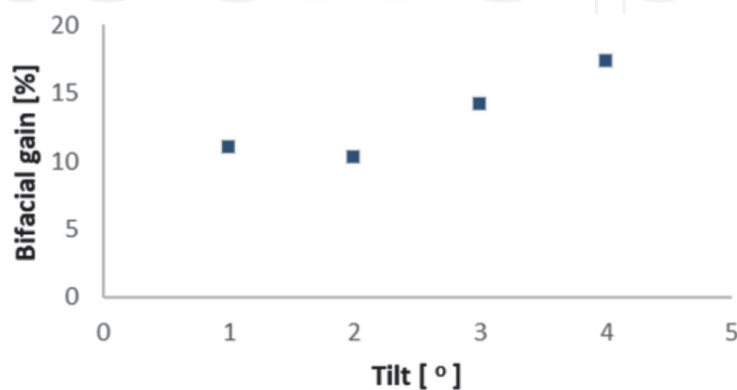


**Figure 8.**

*Bifacial gain as a function of the location with a certain latitude and a tilt angle equal to the latitude.*

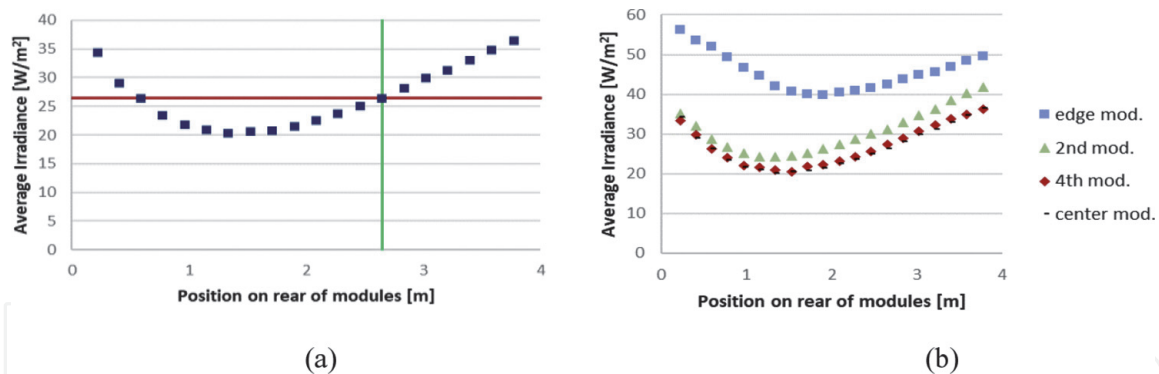


**Figure 9.**

*(a) Position dependence of rear side irradiance, where the 0-meter position corresponds to the bottom of 4 modules and the 4-meter position to the top of 4 modules. The red line corresponds to the average incident irradiance on the PV module and the green line corresponds to the 68% position, and (b) Position dependence of rear side irradiance as a function of PV plant position (edge, 2<sup>nd</sup>, 4<sup>th</sup>, and center-mounted bifacial PV modules).*

The results from selected points in **Figure 9a** are summarized in **Table 4**. As observed in **Table 4**, the pyranometer reading at the 68% position is matched with the average incident irradiance on the PV module. An additional point close to the bottom of the PV module would also be matched, but this point was not chosen since the curve shown in **Figure 9b** is much steeper, which may lead to greater uncertainty.

The results of position effects are shown in **Figure 9b**, where the POA<sup>rear</sup> was plotted at the edge of a row of PV modules and at a set of positions closer to the center of the row. As shown in **Figure 9b**, at the 4<sup>th</sup> module in the row there is practically the same amount of irradiance on the rear of the PV module compared to the modules located at the center. **Figure 10** shows the position dependence of rear



Position [%]	$E_{\text{pyranometer}} - \bar{E}$ [%]	Position [%]	$E_{\text{pyranometer}} - \bar{E}$ [%]
3	+ 30	68	0
23	-18	83	+18
48	-19	98	+38

**Table 4.**  
 Results of the effect of pyranometer position on measured yearly average  $POA^{\text{rear}}$ .

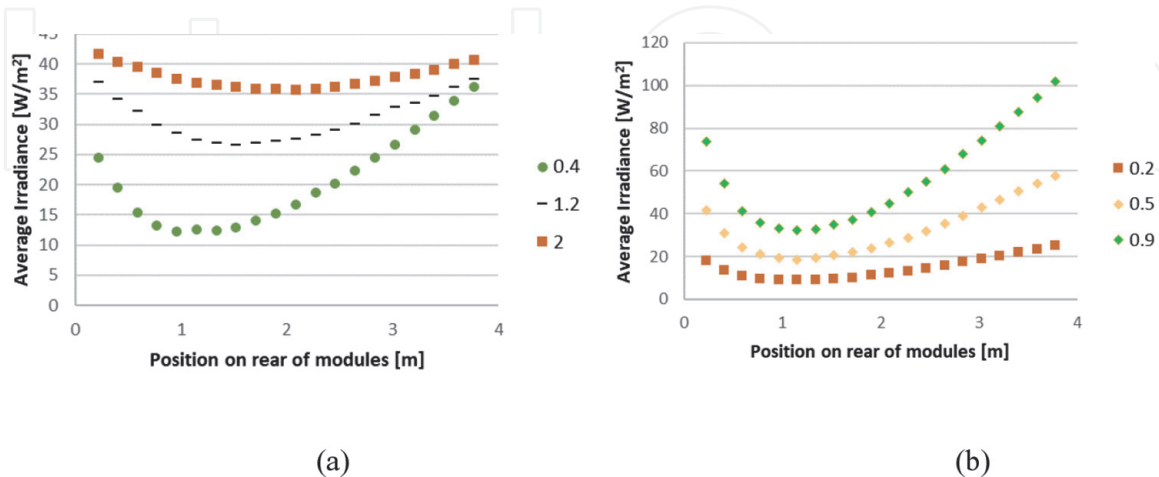


**Figure 10.**  
 (a) Position dependence of rear-side irradiance as a function of clearance height (0.4, 1.2, and 2), and (b) Position dependence of rear-side irradiance as a function of albedo (0.2, 0.5, and 0.9).

side irradiance as a function of clearance and albedo. As observed in **Figure 10**, the best position for measuring  $POA^{\text{rear}}$  irradiance (using a pyranometer) is to be placed sufficiently away from the edge of a row. In this context, when excluding the PV module on the edge side, the shape of  $POA^{\text{rear}}$  only is slightly changed for different positions in the PV plant. Therefore, we considered a 68% position given a value corresponding to the irradiance average of the rear side of the bifacial PV module.

The variation of  $POA^{\text{rear}}$  irradiance for different clearance heights is shown in **Figure 10a**, from a higher clearance height that led to a larger amount of irradiance on the rear side of the PV module. As illustrated in **Figure 10a**, the  $POA^{\text{rear}}$  irradiance is considerably changed when the clearance height is increased from 0.4 meters to 2 meters.

The variation of  $POA^{\text{rear}}$  irradiance for different albedos is shown in **Figure 10b**. As expected, a higher albedo led to a greater irradiance on the rear side of the PV module. The  $POA^{\text{rear}}$  irradiance does not change noticeably over the range of albedos from 0.2 to 0.9. However, the results show that 68% position gives a reasonable average.

The results for tilt, location, and different positions in the PV plant are shown in **Figure 11**. We have considered different locations, namely, Amsterdam in the Netherlands, Yinchuan in China, Salvador in Brazil, and Riyadh in Saudi Arabia. PV strings have been located in different tilt angles in the selected locations, hence there is a moderate variation in the rear side irradiance magnitude, and also in the shape of the distribution. Therefore, the optimum position of the irradiance sensor should not be strongly dependent on the location of the PV plants.

**Figure 12** shows the results for a particular period of the year, certain weather conditions, and different seasons. The results show that the influence of different weather conditions is mostly in the magnitude of the  $POA^{\text{rear}}$  irradiance and less in the shape of the irradiance distribution (see **Figure 12a**). For cloudy and semi-cloudy weather conditions, there is more diffuse and less global irradiance in

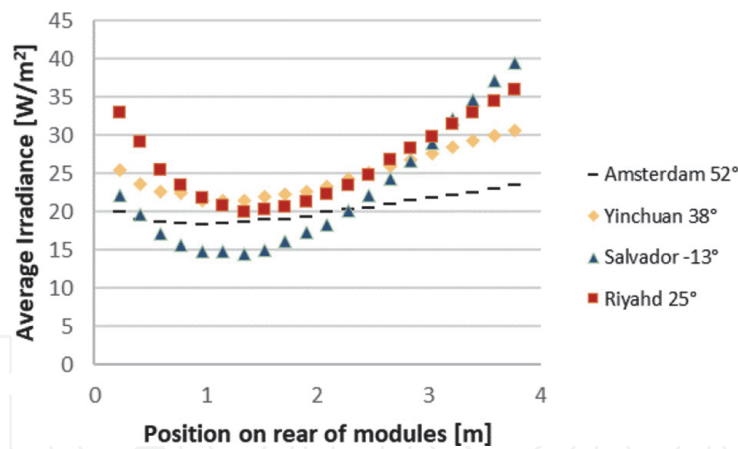


**Figure 11.** Position dependence of rear-side irradiance as a function of location and corresponding optimal tilt angles.

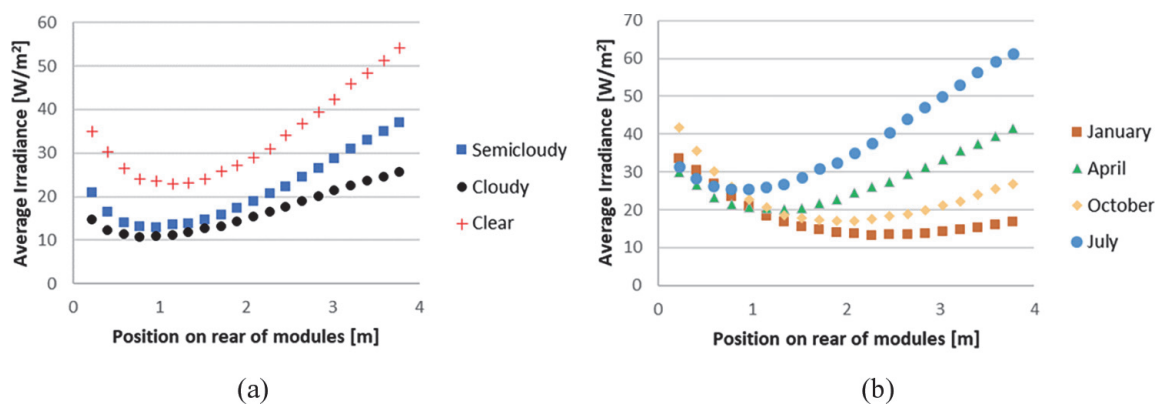


**Figure 12.** (a) Position dependence of rear-side irradiance as a function of weather conditions, (b) Position dependence of rear-side irradiance as a function of season.

comparison with a clear sky, which explains the difference in magnitude of  $POA^{rear}$  irradiance.

As shown in **Figure 12b**, different seasons significantly influence the shape of  $POA^{rear}$  irradiance. For April and July, there is the same amount of irradiance on the rear side of the PV module compared to other ones. However, for higher positions, greater  $POA^{rear}$  irradiance on the rear side of the PV module in July and April compared to October and January. This is most likely influenced by the change in solar zenith angle for these months, and to a lesser extent by the change in weather conditions for the months of April and July. Furthermore, when looking at the seasonal data as shown in **Figure 12b**, the irradiance is changed with the season variations. This will have an impact on the optimal mounting position based on the monthly data.

**Table 5** presents the results of the difference between measuring at a position of 68% from the rear side and the average irradiance on the PV module for variation of the different parameters. In other words, this would be the average  $POA^{rear}$  irradiance difference measured by a pyranometer mounted on the bottom side at the position of 68%. This scores well for changing albedo, height, interplant position, and tilt. For changes in weather and season that are only for a particular period of the year, the 68% position is less representative. This is due to only a particular zenith angle range over a certain (short) period. Strategies for handling this situation can be accepted for a higher measurement uncertainty when looking at the smaller time periods than a year, or alternatively by placing multiple pyranometers at different positions on the rear side of PV modules.

Varied parameter	$ E^{68\%}-\bar{E} $	Varied parameter	$ E^{68\%}-\bar{E} $
Interplant position	1.3 %	tilt/location	5.3%
Albedo	2.8 %	Weather	13%
Height	5.6 %	Season	16%

**Table 5.**  
 Results of difference between irradiance measured at 68% position and average irradiance for parameter variation.

## 5. Performance measurement of bifacial PV modules

We performed some experimental measurements for validation of the irradiance distribution on the back of a bifacial PV module at the Kipp & Zonen roof. To be able to choose the optimal sensor(s) and their position(s) for the  $POA^{rear}$  irradiance measurement, the simulations need to be compared to data from a real-world measurement setup. This setup needs to provide  $POA^{rear}$  sensor data at multiple module height positions as well as the irradiance contribution from the backside of the bifacial module from the total measured module signal. A setup of three rows was constructed where the first row was made of dummy modules for shading, the second middle row contained the modules and sensors, and the third row consisted entirely of modules to simulate proper reflection (as shown in **Figure 13a**). To measure the position-dependent  $POA^{rear}$ , there are 6 Kipp & Zonen CMP11 and 6 SPLite 2 pyranometers mounted next to the rear of one of three bifacial modules (**Figure 13b**).

The collected data from the six sensors were compared to simulations done in the Bifacial Radiance software. In **Figure 14**, the simulation model fits well with the measured data from the experimental setup.

The sensor output needs to be compared to the contribution from the  $POA^{rear}$  signal of the bifacial PV module. Separating the rear side contribution from the total incident irradiance on the PV module was achieved using different methods, each having various following challenges:

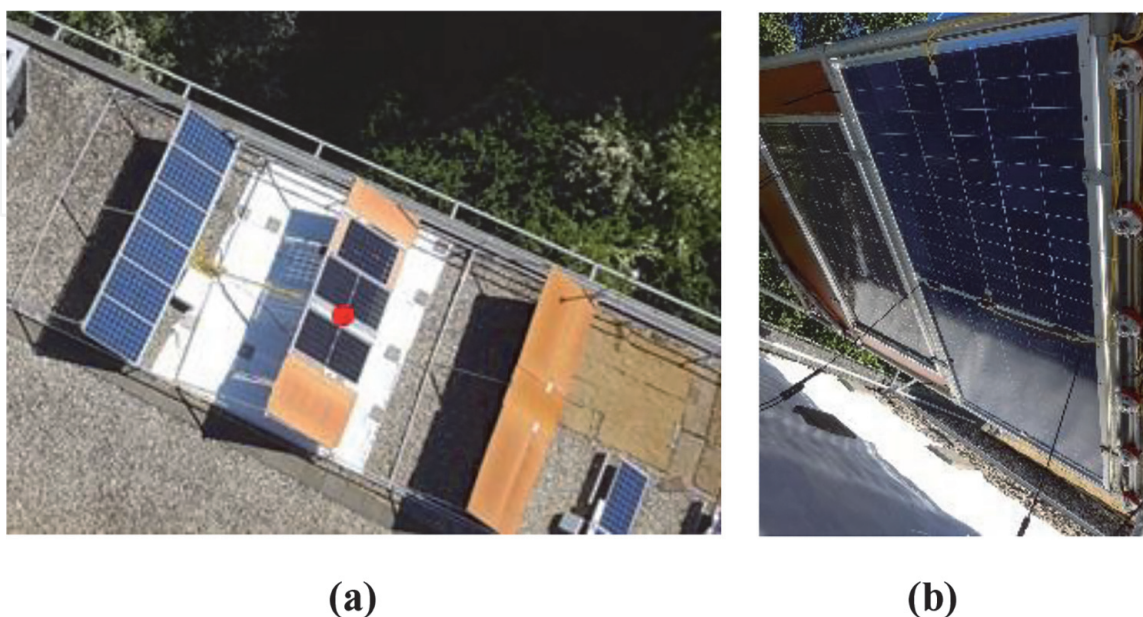


**Figure 13**  
 (a) Top view of Kipp & Zonen module set up in three rows with two types of bifacial modules above a white albedo surface, and (b) row of six CMP11 pyranometers for position-dependent irradiance measurements on the rear module (red dot in (a)).

1. Covering the front side of the bifacial PV module—module logs only  $POA^{rear}$  irradiance.
2. Covering the rear side of one bifacial PV module—module logs only POA irradiance. Subtracting the measured POA irradiance on the first module from the second uncovered module.
3. Using a monofacial PV module with oriented  $POA^{rear}$  irradiance.
4. Measuring the POA and  $POA^{rear}$  ratio with irradiance sensors and applying it to the PV module output.

It needs to be noted that the PV module output was measured as short-circuit current.

## 5.1 Bifacial PV module: $POA^{rear}$ signal separation methods

### 5.1.1 Front side of bifacial PV module ( $POA$ irradiance) covered

This method allows for an easy cut-out of the POA signal, the realization is observed in **Figure 15a**. The major drawback is that it casts a uniform shadow on the ground without light leaking through the solar cells. The difference between a uniform and representative shadow was measured by placing two irradiance sensors on the ground in the shadow and measuring with the covered and uncovered PV module. The difference is 26–29% less irradiance in case of the uniform shadow. This illustrates the effect of a representative shadow, the influence on the  $POA^{rear}$  sensors that would be less than on the ground. This impact is more profound on the measured  $POA^{rear}$  compared to the closer setup in the ground (0.5 m tested) and the higher the albedo, as depicted in **Figure 15b**.

### 5.1.2 Rear side of bifacial PV module ( $POA^{rear}$ irradiance) covered

As shown in **Figure 15b**, we have covered the rear side of the bifacial PV module. The idea behind this concept was to measure the POA irradiance from one module by covering its rear side. This POA irradiance data were then subtracted from the adjacent module, giving the  $POA^{rear}$  irradiance. This method assumes the POA is the same in both modules, although uncertainty may arise from imperfect rear side covering, differences between modules, and slight differences in module mounting angle, which led to acquiring different POA irradiance signal.

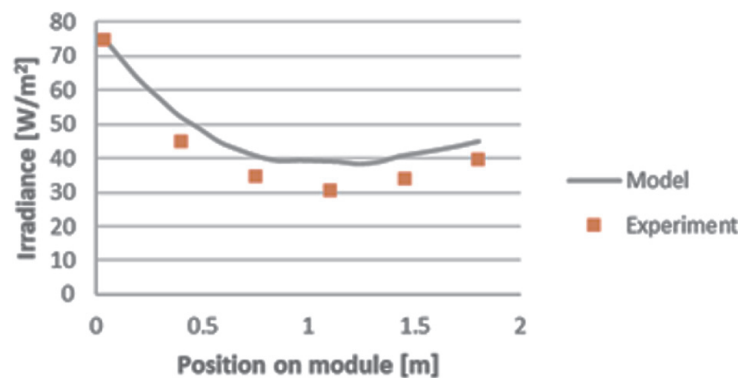


**Figure 14.** Measured experimental data from six pyranometers are compared to the simulated model in Bifacial Irradiance software as a function of height along the module.



**Figure 15.**  
 (a) Measuring  $POA^{rear}$  irradiance with the front side coverage of the PV module, and (b) Measuring POA irradiance with the rear side coverage of the PV module. This is then subtracted from the output of the second uncovered module.

Furthermore, one module is still covered, which casts a uniform shadow. During the day, this shadow extends under another module (from which  $POA^{rear}$  will be extracted), reducing the amount of irradiance on its rear side would be absorbed in comparison with the situation of the uncovered PV module.

### 5.1.3 Monofacial PV module with oriented $POA^{rear}$ irradiance

This method is like the previous method, the advantage being the simplicity of the experiment and set up to get the  $POA^{rear}$  irradiance. The monofacial module needs to be a glass-glass module to let light pass through the solar cells to create a representative shadow and similar heating of the module as in case of a bifacial one.

### 5.1.4 POA and $POA^{rear}$ irradiance sensor ratio applied to the PV module output

The POA and  $POA^{rear}$  irradiance are summed up and calculated. This ratio in percentage is applied to the bifacial PV module output. This method suffers the least from the uniform shadow effect. Errors come from the spectral mismatch of the sensors mounted on the front and rear sides of the module.

Among the aforementioned four methods, we have chosen method 2. Method 3 seemed the best but was not used due to the unavailability of monofacial glass-glass modules at the time. The contribution of rear side of the PV module was calculated through Eq. (10).

$$POA_{rearRelative} \approx \frac{BifacialPanel - BifacialPanelBackCovered}{BifacialPanel \times \Phi_{ISC}} \quad (10)$$

where  $\Phi_{ISC}$  is the module bifaciality factor for short-circuit current. To make a fair comparison with the sensors, both POA and  $POA^{rear}$  from each sensor are needed. Each sensor was calibrated on the POA side before being turned around to measure  $POA^{rear}$ . Having the relative  $POA^{rear}$  contribution from module and sensors, the difference of the sensors to the module  $POA^{rearRelative}$  is calculated:

$$POA_{rearRelative} = \frac{POA_{rear}}{POA + POA_{rear}} \quad (11)$$

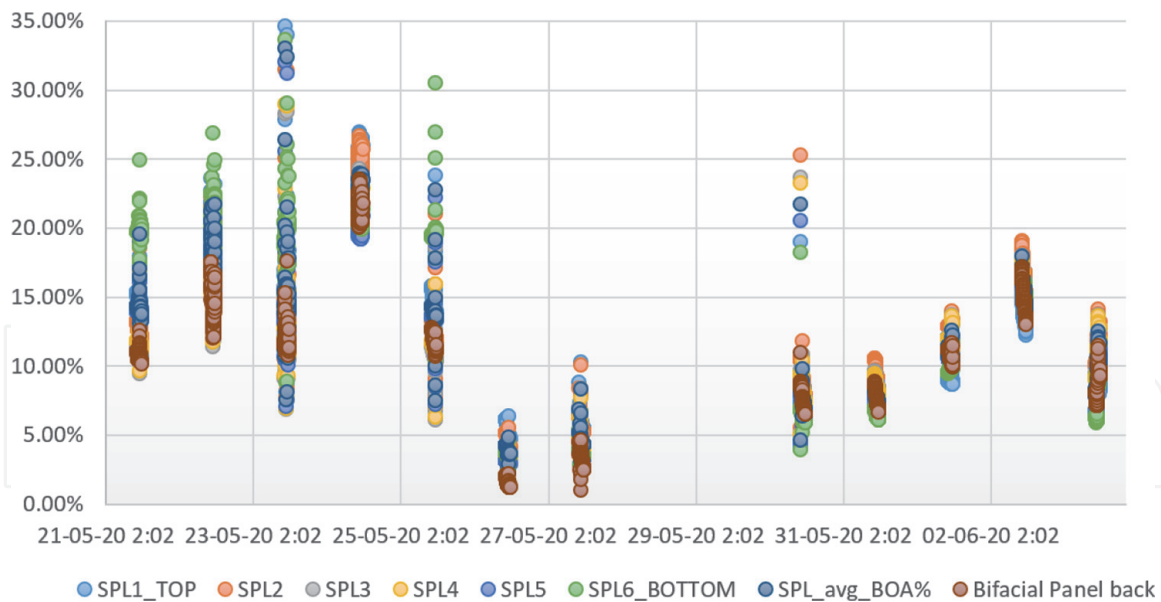


**Figure 16.**

The comparison of SP Lite2 irradiance sensors and the bifacial module in  $POA^{rearRelative}$  under various tilt angles, surface coverages, and weather conditions (only data between 12:00 and 13:30 local time has been considered).

This method is extremely dependent on the accuracy of the POA irradiance sensors. The POA sensors need to be leveled and oriented precisely as same as the orientation of the module. Even more critical, the two PV modules need to be perfectly aligned; otherwise, their relative performance is changed as the sun moves over the day.

In this study, only data from 12:00 to 13:30 local time from each day has been used. This is due to the POA irradiance sensor error mentioned above and due to shadowing from surrounding structures outside of these hours.

## 5.2 $POA^{rear}$ irradiance on module and sensor comparison

Data were taken from the setup having various module tilt angles ( $30^\circ$ ,  $45^\circ$ , and  $60^\circ$ ) ground covers (white fleece, artificial grass, and roof stones) and experiencing various weather conditions. Generally, the  $POA^{rear}$  irradiance contributions are higher during cloudy and overcast weather compared to sunny conditions (see **Figure 16**). This is due to a significant reduction in POA contribution. The highest  $POA^{rear}$  contributions are obtained at the lowest angle ( $30^\circ$ ) and highest albedo using the white fleece (days from 21-5-20 to 25-5-20; see again **Figure 16**). The sensor readings have a higher spread during sunny weather conditions due to the higher direct light contribution, as on the day of 23-5-20 (see again **Figure 16**). The lowest sensor (#6) receives the most irradiance because of higher incident direct light on it compared to other sensors. In cloudy weather conditions, there is only diffuse irradiation, so the spread of the sensor's output is narrow (day 24-5-20; see again **Figure 16**). This is also the case at the highest setup tilt angle ( $60^\circ$ ) where the effect of direct reflected irradiation is reduced (from day 30-5-20 onwards; see again **Figure 16**). Pyranometers at positions 3 and 4 (60% and 40% of height of module) have the best overlap with the module data.

## 6. Discussion and conclusions

In recent decades, photovoltaics (PV) technology has received more attention and PV installation is being dramatically deployed. The PV capacity is being

approached to one Tera Watt (TWp) in the world. A novel development is the advent of bifacial PV modules that enhance energy production by converting incident irradiance on the rear side of module into electricity. In this chapter, we discussed the physics principle and applications of bifacial PV technology. As discussed, PV plant design considerations influence the bifacial gain. Furthermore, an expected linear relation between the albedo and the bifacial gain was demonstrated in this chapter. Moreover, we proved that mounting the modules at higher heights has a large effect compared to the installed module at a lower height, but once the modules are mounted more than 1.5 meters from the ground, the effect was reduced. To improve the bifacial gain for a particular site, the design of PV strings should be considered by selecting a site with a higher albedo or increasing the albedo artificially by terraforming, for example, using white fleece or stones as ground cover, or regularly moving the vegetation.

We have also discussed that besides the PV plant design, the location and weather conditions play a vital role in the bifacial gain. As shown, at higher latitudes, where corresponding larger tilt angles are used the bifacial gain has been increased. This is most likely caused by the larger tilt of the modules, which ensures that more diffuse irradiance can be absorbed by the rear side of PV modules as well as more soil that scatters direct irradiance from the sun.

In cloudy weather conditions, bifacial gains have been increased, most likely because cloudy conditions tend to have a larger diffuse component in the sky irradiance compared to clear conditions. In addition to that, the direct component in cloudy conditions was decreased thereby significantly reducing the front side irradiance on the PV module. Therefore, it can be said that in the locations with higher tilt angles as well as more cloudy weather, the position percentage is increased in power output by installing bifacial modules instead of monofacial ones that are greater than for lower tilt angles and clear weather.

However, as clear weather and lower tilt angles (latitudes) promote a higher absolute energy generation, the kilowatt-hour (kWh) gain might be larger in clear weather and lower latitudes as opposed to larger latitudes or cloudy conditions.

It should also be mentioned that there is a seasonal component to the bifacial gain, namely, in the summer months there is a larger bifacial gain than in the winter months. This is most likely due to the increasing irradiance of the land close to the modules with higher sun angles as it is typical in the summertime. In this way, the  $POA^{\text{rear}}$  irradiance of the module is increased as more light scatters from the surface to the rear side of the bifacial PV module.

In summary, in this chapter, we also presented the advantages and performance measurements of bifacial PV technologies. We discussed the recent characterization techniques of bifacial PV modules. Furthermore, for accurately knowing the performance ratio of PV strings with bifacial modules, we explained how to measure the irradiance due to ground albedo. This can be performed with either an albedometer or the front and rear-side plane of array (POA) irradiance very accurately.

By means of simulation using Bifacial Radiance software developed by NREL, we investigated insight into what boundary conditions result in new bifacial technology gains and the influence of the mounting position of irradiance sensors. To this end, we performed different experiments by varying the sensor positions on the rear side of the PV modules in different locations within the PV plant, different albedo numbers, mounting heights, as well as different geographical locations with different tilts, different seasons, and weather types, are investigated. Validation of the results of the simulation using multiple sensors in the Kipp & Zonen roof setup was presented.

Simulation results demonstrated that the irradiance on the rear side of the PV modules varies strongly with its positions. The results also proved that the rear side

irradiance distribution and magnitude were varied with albedo, clearance height, and tilt. For the plant of four landscape-positioned modules above each other, an installation position on the rear side of the module at approximately 68% represented the average irradiance well in case of cumulative yearly results. We recommend that for other designs a similar optimal position for yearly results can be found but at a slightly different position.

According to the results, we advise to install the POA<sup>rear</sup> sensor (s) significantly away from the start or end of a string. Seasonal results or results for a day with weather showed significant changes in the rear side irradiance pattern, impacting the optimal sensor position for seasonal analysis. A possible mitigation strategy is to use multiple pyranometers at different positions.

## Author details

Mohammadreza Aghaei<sup>1\*</sup>, Marc Korevaar<sup>2,3</sup>, Pavel Babal<sup>2,3</sup> and Hesam Ziar<sup>4</sup>

1 Department of Ocean Operations and Civil Engineering, Norwegian University of Science and Technology (NTNU), Alesund, Norway


2 Kipp and Zonen, Delft, The Netherlands

3 OTT Hydromet B.V., Kempten, Germany

4 Delft University of Technology (TU Delft), Photovoltaic Materials and Devices, Delft, Netherlands

\*Address all correspondence to: mohammadreza.aghaei@ntnu.no

## IntechOpen

© 2022 The Author(s). Licensee IntechOpen. This chapter is distributed under the terms of the Creative Commons Attribution License (<http://creativecommons.org/licenses/by/3.0>), which permits unrestricted use, distribution, and reproduction in any medium, provided the original work is properly cited. 



## References

- [1] Available from: <https://www.pv-magazine.com/2022/03/15/humans-have-installed-1-terawatt-of-solar-capacity/> (n.d.)
- [2] Guerrero-Lemus R, Vega R, Kim T, Kimm A, Shephard LE. Bifacial solar photovoltaics – A technology review. *Renewable and Sustainable Energy Reviews*. 2016;**60**:1533-1549
- [3] Aghaei M, Nitti M, Ekins-Daukes NJ, Reinders AHME. Simulation of a novel configuration for luminescent solar concentrator photovoltaic devices using bifacial silicon solar cells. *Applied Sciences*. 2020;**10**(3):1-10. DOI: 10.3390/app10030871
- [4] Aghaei M, Pelosi R, Wong WWH, Schmidt T, Debije MG, Reinders AHME. Measured power conversion efficiencies of bifacial luminescent solar concentrator photovoltaic devices of the mosaic series. *Progress in Photovoltaics Research and Applications*. 2022:1-14. DOI: 10.1002/pip.354614AGHAEIET AL
- [5] Aghaei M, Zhu X, Debije MG, Wong WWH, Schmidt T, Reinders AHME. Simulations of Luminescent Solar Concentrator Bifacial Photovoltaic Mosaic Devices Containing Four Different Organic Luminophores. *IEEE Journal of Photovoltaics*. 2022;**3**(3): 771-777. DOI: 10.1109/JPHOTOV.2022.3144962
- [6] Luque A, Cuevas A, Ruiz J. Double-sided n<sup>+</sup>-p-n<sup>+</sup> solar cell for bifacial concentration. *Solid Cells*. 1980;**2**(2): 151-166
- [7] Hiroshi M. Radiation energy transducing device. In: Google Patents. 1966
- [8] Liang TS et al. A review of crystalline silicon bifacial photovoltaic performance characterisation and simulation. *Energy & Environmental Science*. 2019;**12**:116-148. DOI: 10.1039/c8ee02184h
- [9] Chambouleyron I, Chevalier Y. Silicon double solar cell. In: *Photovoltaic Solar Energy Conference*. 1978. pp. 967-976
- [10] Cuevas A, Luque A, Eguren J, Del Alamo J. High efficiency bifacial back surface field solar cells. *Solid Cells*. 1981;**3**(4):337-340
- [11] Cuevas A, Luque A, Eguren J, del Alamo J. 50 Per cent more output power from an albedo-collecting flat panel using bifacial solar cells. *Solar Energy*. 1982;**29**(5):419-420
- [12] Luque A, Lorenzo E, Sala G, López-Romero S. Diffusing reflectors for bifacial photovoltaic panels. *Solid cells*. 1985;**13**(3):277-292
- [13] Hezel R. Novel applications of bifacial solar cells. *Progress in Photovoltaics: Research and Applications*. 2003;**11**(8):549-556
- [14] Halm A et al. Encapsulation losses for ribbon contacted N-type IBC solar cells. In: *29th European Photovoltaic Solar Energy Conference and Exhibition (EU PVSEC 2014)*. 2014. pp. 190-193. DOI: 10.4229/EUPVSEC20142014-1BV.6.49
- [15] Kreinin L, Bordin N, Karsenty A, Drori A, Eisenberg N. Experimental analysis of the increases in energy generation of bifacial over mono-facial PV modules. In: *Proceedings of the 26th Europe Photovoltaic Solar Energy Conference Exhibition*. Hambourg, Genmany; 2011. pp. 5-9
- [16] Hauser A, Richter A, Leu S. Cell and Module Design from the LCOE Perspective. *Semantic Scholar*. Meyer Burg; 2014. <https://www.semanticscholar.org/>

- olar.org/paper/Cell-and-module-design-from-the-LCOE-perspectiveHauser/af0969f73251b9424a91bcd5c17c42a164e2a200
- [17] Chiodetti M. Bifacial PV plants: Performance model development and optimization of their configuration. Sweden: KTH Royal Institute of Technology; 2015
- [18] Sugibuchi K, Ishikawa N, Obara S. Bifacial-PV power output gain in the field test using 'EarthON' high bifaciality solar cells. In: Proc. 28th PVSEC. 2013. pp. 4312-4317
- [19] Yang L et al. High efficiency screen printed bifacial solar cells on monocrystalline CZ silicon. *Progress in Photovoltaics: Research and Applications*. 2011;**19**(3):275-279
- [20] Dullweber T et al. PERC+: Industrial PERC solar cells with rear Al grid enabling bifaciality and reduced Al paste consumption. *Progress in Photovoltaics: Research and Applications*. 2016;**24**(12):1487-1498
- [21] Hübner A, Aberle AG, Hezel R. Novel cost-effective bifacial silicon solar cells with 19.4% front and 18.1% rear efficiency. *Applied Physics Letters*. 1997;**70**(8):1008-1010
- [22] Aberle AG, Glunz S, Warta W. Impact of illumination level and oxide parameters on Shockley-Read-Hall recombination at the Si-SiO<sub>2</sub> interface. *Journal of Applied Physics*. 1992;**71**(9): 4422-4431
- [23] Solar World. Calculating the additional energy yield of bifacial solar modules. Available from: <https://solarenpower.com/pdf/Calculating-Additional-Energy-Yield-Through-Bifacial-Solar-Technology.pdf>
- [24] Lohmüller E et al. Bifacial p-type silicon PERL solar cells with screen-printed pure silver metallization and 89% bifaciality. In: 33rd EU PVSEC. 2017. pp. 418-423
- [25] Green MA, Blakers AW, Zhao J, Milne AM, Wang A, Dai X. Characterization of 23-percent efficient silicon solar cells. *IEEE Transactions on Electron Devices*. 1990;**37**(2):331-336
- [26] Tool CJJ et al. Industrial cost effective N-PASHA solar cells with ampersand >20% efficiency. *ECN*. 2013
- [27] Cai W et al. 22.2% efficiency n-type PERT solar cell. *Energy Procedia*. 2016; **92**:399-403
- [28] Wei Q, Zhang S, Yu S, Lu J, Lian W, Ni Z. High efficiency n-PERT solar cells by B/P co-diffusion method. *Energy Procedia*. 2017;**124**:700-705
- [29] Ishikawa N. Industrial production of high efficiency and high bifaciality solar cells. 2012. [Online]. Available: <https://pvpmc.sandia.gov/resources-and-events/events/2012-bifacial-pv-workshop-konstanz/>
- [30] Galbiati G, Chu H, Mihailetchi VD, Libal J, Kopecek R. Latest results in screen-printed IBC-ZEBRA solar cells. In: 2018 IEEE 7th World Conference on Photovoltaic Energy Conversion (WCPEC) (A Joint Conference of 45th IEEE PVSC, 28th PVSEC & 34th EU PVSEC). 2018. pp. 1540-1543
- [31] Kopecek R et al. Bifaciality: One small step for technology, one giant leap for kWh cost reduction. *Photovoltaics Institute*. 2014;**26**:32-45
- [32] Halm A et al. The zebra cell concept-large area n-type interdigitated back contact solar cells and one-cell modules fabricated using standard industrial processing equipment. In: Proc. the 27th EU Photovoltaic Specialists Conference. 2012. pp. 567-570
- [33] Galbiati G et al. "Large-area back-contact back-junction solar cell with

- efficiency exceeding 21%,” in 2012 IEEE 38th Photovoltaic Specialists Conference (PVSC) PART 2. 2012. pp. 1–6.
- [34] Cesar I et al. Enablers for IBC: Integral cell and module development and implementation in PV industry. *Energy Procedia*. 2017;124:834-841
- [35] Mewe A et al. Mercury: Industrial IBC cell with front floating emitter for 20.9% and higher efficiency. In: 2015 IEEE 42nd Photovoltaic Specialist Conference (PVSC). 2015. pp. 1-6
- [36] Taguchi M et al. 24.7% record efficiency HIT solar cell on thin silicon wafer. *IEEE Journal of Photovoltaics*. 2013;4(1):96-99
- [37] Janssen GJM et al. Minimizing the polarization-type potential-induced degradation in PV modules by modification of the dielectric antireflection and passivation stack. *IEEE Journal of Photovoltaics*. 2019; 9(3):608-614. DOI: 10.1109/JPHOTOV.2019.2896944
- [38] Kinoshita EMT, Fujishima D, Yano A, Ogane A, Tohoda S, Matsuyama K, et al. The approaches for high efficiency HITTM solar cell with very thin (<100  $\mu\text{m}$ ) silicon wafer over 23% 2011. pp. 871-874
- [39] Paper W. Heterojunction Technology. 2015. Available from: <https://www.meyerburger.com/sg/en/meyer-burger/media/multimedia/publications/article/heterojunction-technology-the-solar-cell-of-the-future/>
- [40] Ghozati SB, Ebong AU, Honsberg CB, Wenham SR. Improved fill-factor for the double-sided buried-contact bifacial silicon solar cell. *Solar Energy Materials & Solar Cells*. 1998;51(2):121-128
- [41] Wenham SR, Chan BO, Honsberg CB, Green MA. Beneficial and constraining effects of laser scribing in buried-contact solar cells. *Progress in Photovoltaics: Research and Applications*. 1997;5(2):131-137
- [42] Ebong AU, Lee SH, Honsberg C, Wenham SR. High efficiency double sided buried contact silicon solar cells. *Japanese Journal of Applied Physics*. 1996;35(4R):2077
- [43] Verlinden PJ et al. Sliver® solar cells: A new thin-crystalline silicon photovoltaic technology. *Solar Energy Materials & Solar Cells*. 2006; 90(18–19):3422-3430
- [44] Weber K, Everett V, Franklin E, Blakers A. Results of a Cost Model for Sliver Cells. 2006
- [45] Untila GG et al. Bifacial concentrator Ag-free crystalline n-type Si solar cell. *Progress in Photovoltaics: Research and Applications*. 2015;23(5):600-610
- [46] Metz A, Fischer M, Trube J. “Recent results of the international technology roadmap for photovoltaics (ITRPV).” ITRPV, 2017
- [47] Bristow KL. On solving the surface energy balance equation for surface temperature. *Agricultural and Forest Meteorology*. 1987;39(1):49-54
- [48] Idso SB, Jackson RD, Reginato RJ, Kimball BA, Nakayama FS. The dependence of bare soil albedo on soil water content. *Journal of Applied Meteorology and Climatology*. 1975; 14(1):109-113
- [49] Matthias AD et al. Surface roughness effects on soil albedo. *Soil Science Society of America Journal*. 2000;64(3):1035-1041
- [50] Taha H. Urban climates and heat islands: Albedo, evapotranspiration, and anthropogenic heat. *Energy and Buildings*. 1997;25(2):99-103
- [51] Kirn B, Brecl K, Topic M. A new PV module performance model based on

separation of diffuse and direct light. *Solar Energy*. 2015;**113**:212-220

[52] Calcabrini A, Ziar H, Isabella O, Zeman M. A simplified skyline-based method for estimating the annual solar energy potential in urban environments. *Nature Energy*. 2019;**4**(3):206-215

[53] Wood Mackenzie. Global bifacial module market report 2019. 2020. [Online]. Available: <https://www.woodmac.com/reports/power-markets-global-bifacial-module-market-report-2019-348173>

[54] Brennan MP, Abramase AL, Andrews RW, Pearce JM. Effects of spectral albedo on solar photovoltaic devices. *Solar Energy Materials & Solar Cells*. 2014;**124**:111-116

[55] Russell TCR, Saive R, Augusto A, Bowden SG, Atwater HA. The influence of spectral albedo on bifacial solar cells: A theoretical and experimental study. *IEEE Journal of Photovoltaics*. 2017;**7**(6):1611-1618

[56] Liang S, Zhang X, He T, Cheng J, Wang D. Remote sensing of the land surface radiation budget. *Remote Sens. energy fluxes soil moisture content*. 2013:121-162

[57] He T, Liang S, Yu Y, Wang D, Gao F, Liu Q. Greenland surface albedo changes in July 1981–2012 from satellite observations. *Environmental Research Letters*. 2013;**8**(4):44043

[58] Loarie SR, Lobell DB, Asner GP, Mu Q, Field CB. Direct impacts on local climate of sugar-cane expansion in Brazil. *Nature Climate Change*. 2011;**1**(2):105-109

[59] Offerle B, Jonsson P, Eliasson I, Grimmond CSB. Urban modification of the surface energy balance in the West African Sahel: Ouagadougou, Burkina Faso. *Journal of Climate*. 2005;**18**(19):3983-3995

[60] Govaerts Y, Lattanzio A. Estimation of surface albedo increase during the eighties Sahel drought from Meteosat observations. *Global and Planetary Change*. 2008;**64**(3–4):139-145

[61] Seneviratne SI et al. Land radiative management as contributor to regional-scale climate adaptation and mitigation. *Nature Geoscience*. 2018;**11**(2):88-96

[62] Ziar H, Sönmez FF, Isabella O, Zeman M. A comprehensive albedo model for solar energy applications: Geometric spectral albedo. *Applied Energy*. 2019;**255**:113867

[63] Kipp & Zonnen BV. *Albedometers*. 2015

[64] Sönmez FF, Ziar H, Isabella O, Zeman M. Fast and accurate ray-casting-based view factor estimation method for complex geometries. *Solar Energy Materials & Solar Cells*. 2019;**200**:109934

[65] NASA. Moderate Resolution Imaging Spectrometer. 2022. <https://modis.gsfc.nasa.gov>

[66] He T et al. Evaluating land surface albedo estimation from Landsat MSS, TM, ETM+, and OLI data based on the unified direct estimation approach. *Remote Sensing of Environment*. 2018;**204**:181-196

[67] Lucht W, Schaaf CB, Strahler AH. An algorithm for the retrieval of albedo from space using semiempirical BRDF models. *IEEE Transactions on Geoscience and Remote Sensing*. 2000;**38**(2):977-998

[68] Enriquez R, Zarzalejo L, Jiménez MJ, Heras MR. Ground reflectance estimation by means of horizontal and vertical radiation measurements. *Solar Energy*. 2012;**86**(11):3216-3226

- [69] Psiloglou BE, Kambezidis HD. Estimation of the ground albedo for the Athens area, Greece. *Journal of Atmospheric and Solar—Terrestrial Physics*. 2009;**71**(8–9):943-954
- [70] Liu BYH, Jordan RC. The long-term average performance of flat-plate solar-energy collectors: With design data for the US, its outlying possessions and Canada. *Solar Energy*. 1963;**7**(2):53-74
- [71] Ineichen P, Perez R, Seals R. The importance of correct albedo determination for adequately modeling energy received by tilted surfaces. *Solar Energy*. 1987;**39**(4):301-305
- [72] Gueymard C. Mathematically integrable parameterization of clear-sky beam and global irradiances and its use in daily irradiation applications. *Solar Energy*. 1993;**50**(5):385-397
- [73] Nkemdirim LC. A note on the albedo of surfaces. *Journal of Applied Meteorology*. 1972;**11**(5):867-874
- [74] Ineichen P, Guisan O, Perez R. Ground-reflected radiation and albedo. *Solar Energy*. 1990;**44**(4):207-214
- [75] Hay JE. Calculating solar radiation for inclined surfaces: Practical approaches. *Renewable Energy*. 1993;**3**(4–5):373-380
- [76] Temps RC, Coulson KL. Solar radiation incident upon slopes of different orientations. *Solar Energy*. 1977;**19**(2):179-184
- [77] IEC. Photovoltaic Devices—Part 1-2: Measurement of Current-Voltage Characteristics of Bifacial Photovoltaic (PV) Devices; IEC TS 60904-1-2:2019, IEC TS. 2019
- [78] Deline C, MacAlpine S, Marion B, Toor F, Asgharzadeh A, Stein JS. Assessment of bifacial photovoltaic module power rating methodologies—inside and out. *IEEE Journal of Photovoltaics*. 2017;**7**(2):575-580
- [79] Nussbaumer H et al. Accuracy of simulated data for bifacial systems with varying tilt angles and share of diffuse radiation. *Solar Energy*. 2020; **197**:6-21
- [80] Singh JP, Guo S, Peters IM, Aberle AG, Walsh TM. Comparison of glass/glass and glass/backsheet PV modules using bifacial silicon solar cells. *IEEE Journal of Photovoltaics*. 2015;**5**(3): 783-791
- [81] Razongles G et al. Bifacial photovoltaic modules: Measurement challenges. *Energy Procedia*. 2016;**92**: 188-198
- [82] Corbellini G, Vasco M. Analysis and modelling of bifacial PV modules. In: 14th PV Performance Modeling Collaborative Workshop Modelling of Bifacial PV Modules. 2015
- [83] Singh JP, Aberle AG, Walsh TM. Electrical characterization method for bifacial photovoltaic modules. *Solar Energy Materials & Solar Cells*. 2014; **127**:136-142
- [84] Edler A, Metz A. Need for standardized measurements of bifacial solar cells and PV modules. In: 14th PV Performance Modeling Collaborative Workshop Modelling of Bifacial PV Modules. 2015
- [85] Ezquer M, Petrina I, Cuadra JM, Lagunas A, Cener-Ciemat F. Design of a special set-up for the IV characterization of bifacial photovoltaic solar cells. 2009
- [86] Soria B, Gerritsen E, Lefillastre P, Broquin JE. A study of the annual performance of bifacial photovoltaic modules in the case of vertical facade integration. *Energy Science Engineering*. 2016;**4**:52-68. DOI: 10.1002/ese3.103

[87] Bliss M, Betts TR, Gottschalg R. Indoor measurement of photovoltaic device characteristics at varying irradiance, temperature and spectrum for energy rating. *Measurement Science and Technology*. 2010;21(11):115701

[88] Stuckelberger M et al. Class AAA LED-based solar simulator for steady-state measurements and light soaking. *IEEE Journal of Photovoltaics*. 2014;4(5):1282-1287

[89] Deline C, Marion W, Ayala S. Bifacial Radiance. 2017. Available from: [https://github.com/NREL/bifacial\\_radiance](https://github.com/NREL/bifacial_radiance)

[90] Riedel-Lyngskær N, Petit M, Berrian D, Poulsen PB, Libal J, Jakobsen ML. A spatial irradiance map measured on the rear side of a utility-scale horizontal single axis tracker with validation using open source tools. In: 2020 47th IEEE Photovoltaic Specialists Conference (PVSC). 2020. pp. 1026-1032

[91] Pelaez SA, Deline C, Greenberg P, Stein JS, Kostuk RK. Model and validation of single-axis tracking with bifacial PV. *IEEE Journal of Photovoltaics*. 2019;9(3):715-721

[92] Pelaez SA, Deline C, MacAlpine SM, Marion B, Stein JS, Kostuk RK. Comparison of bifacial solar irradiance model predictions with field validation. *IEEE Journal of Photovoltaics*. 2018;9(1):82-88

[93] Landau CR. Optimum tilt of solar panels. 2014. Available from: <https://www.solarpaneltilt.com/>

[94] NREL. Weather Data. Available from: <https://energyplus.net/weather> [Accessed: 20.01.2020]